https://doi.org/10.5194/egusphere-2023-491
Preprint. Discussion started: 9 May 2023

Implementation of a Simple Actuator Disc for Large Eddy Simulation (SADLES-V1.0) in the Weather Research and Forecasting Model (V4.3.1) for Wind Turbine Wake Simulation

Hai Bui[1,2], Mostafa Bakhoday-Paskyabi[1,2], and Mohammadreza Mohammadpour-Penchah[1,2]

[1]Geophysical Institute, University of Bergen, Allégaten 70, 5007 Bergen, Norway
[2]Bergen Offshore Wind Centre, Allégaten 55, 5007 Bergen, Norway

Correspondence: Hai Bui (hai.bui@uib.no)

Abstract. The development of wind energy in recent years has made the representation of wind turbines in numerical models essential for wind resource and environmental assessment. In this study, we introduce a new wind turbine model, the Simple Actuator Disc for Large Eddy Simulation (SADLES), parameterized in the Weather Research and Forecast (WRF) model. Our goal is to perform realistic downscaling of large eddy simulation, so we integrated SADLES and the cell perturbation method as WRF modules and released the code as open-source for further research. We demonstrate the effectiveness of SADLES by comparing a large eddy simulation of a 5-MW wind turbine using the WRF-SADLES with the Parallelized Large-eddy simulation Model (PALM), showing that SADLES can simulate wind turbine wakes effectively at an intermediate resolution of a few dozen meters. Furthermore, we show the applicability of SADLES in wind farm assessment by downscaling the ERA5 reanalysis data to study turbine-to-turbine and farm-to-farm interactions for the Alpha Ventus wind farm. In our case study, due to the wind farm to the southwest, the ambient wind speed at Alpha Ventus is reduced by 14% and the average turbine power is reduced by 35%. SADLES provides a promising balance between computational efficiency and accuracy for wind turbine wake simulations and has potential applications in wind energy assessment and wind farm construction planning.

1 Introduction

Wind energy has become increasingly important due to the pressing need to address climate change and reduce our reliance on fossil fuels. It is crucial to have a deep understanding of the complex interaction between wind turbines and the atmospheric boundary layer (ABL) for effective wind energy assessment and wind farm construction planning. In particular, the wake created behind upstream turbines can have a significant impact on the performance of downstream turbines, resulting in reduced power production, increased turbulence, and dynamic loading (Porté-Agel et al., 2020; Bakhoday-Paskyabi et al., 2022a). Large eddy simulation (LES) is a powerful tool that can simulate ABL turbulence with high spatial and temporal resolution, making it an invaluable resource for studying turbine wakes and and their interaction with the ABL (Breton et al., 2017).

To model the turbine wakes, various methods can be used to simulate the rotor with varying levels of accuracy and computational cost. The most accurate, but computationally expensive methods are the actuator surface (AS) and actuator line (AL) models, which typically use the blade element method (BEM, Burton et al., 2011; Göçmen et al., 2016) to calculate the thrust

https://doi.org/10.5194/egusphere-2023-491
Preprint. Discussion started: 9 May 2023

and torque acting on the turbine blades. A less computationally expensive method is the actuator disc with rotation (AD+R) model, where the turbine blades are represented by a rotating circular disc that extracts energy from the wind through axial and azimuthal forces. The actuator disc without rotation (AD) is the simplest form, where only the axial force is considered. These methods have been applied in various LES models, such as the EllipSys3D model (Göçmen et al., 2016, AL), the MITRAS model (Salim et al., 2018, AD+R), the Simulator for Wind Farm Applications (SOWFA) (Fleming et al., 2014; Churchfield et al., 2016, AL), and the Parallelized Large-eddy simulation Model (PALM) (Witha et al., 2014; Maronga et al., 2015, 2020, AL, AD, AD+R). For applications that do not require a very high resolution and detailed near wake structures, the AD+R and AD methods are often favorable as they require fewer computational resources, are easier to implement, and yet achieve an adequate level of accuracy for far wake information (Breton et al., 2017)

Besides the accuracy of the turbine wake methods, a realistic ABL plays a crucial role in wake simulations. The processes that affect wind farms range from macro- and meso-scale weather phenomena, such as cyclones and fronts, down to the micro-scale of turbulence in the ABL (Porté-Agel et al., 2020). Given this multi-scale nature, a macro-to-micro numerical downscaling could be useful in simulating the ABL-turbine interaction realistically and understanding its underlying mechanisms. To incorporate realistic ABL conditions, one can use the meso-micro offline coupling approach, i.e. the output of a mesoscale model is used as the driven boundary condition for the dedicated LES models (e.g. Wang et al., 2020; Lin et al., 2021; Bakhoday-Paskyabi et al., 2022b; Onel and Tuncer, 2023). However, this approach depends on the frequency of the mesoscale model output, which is often not enough for short time scale processes. The second approach, online coupling, is using a meso-micro coupled model system, where a mesoscale model and a LES model through a coupling interface. While the online coupling approach provides a seamless downscaling, it is more difficult to implement than the offline approach. The third approach, nested downscaling, is using a single model can handle the downscaling naturally through a system of nested domains where the outer and inner domains can be configured to run in LES mode. For example, the Consortium for Small-scale Modeling (COSMO) model (Baldauf et al., 2011) and the Weather Research and Forecast (WRF) model (Skamarock et al., 2019) provide this capability.

The purpose of this study is to develop a macro-to-micro nested downscaling framework that can simulate turbine wakes with realistic ABL conditions. We chose the WRF model as it is an open-source model widely used by the research community to study a wide range of atmospheric processes, from idealized studies to real-world applications. There are several WRF implementations that include the effects of wind farms and wind turbines (e.g. Fitch et al., 2012; Volker et al., 2015; Mirocha et al., 2014; Kale et al., 2022), which can be grouped into wind farm parameterization (WFP) and wind turbine model (WTM).

The WFP approaches (Fitch et al., 2012; Volker et al., 2015) are commonly used to study the collective effects of wind turbine wakes on the ABL and the interactions between wind farms (e.g. Pryor et al., 2020; Fischereit et al., 2022). One advantage of these approaches is their low computational cost and ease of implementation. For example, (Fitch et al., 2012) only requires the thrust and power curve data from turbine manufacturers. However, due to the limitation of the target horizontal resolutions, which must be at least 3 to 5 rotor diameters (Fischereit et al., 2022), the WFP cannot resolve individual turbine wakes explicitly, nor turbine-to-turbine interactions. This may result in inaccurate evaluations of wakes behind wind farms (Lee and Lundquist, 2017).

https://doi.org/10.5194/egusphere-2023-491
Preprint. Discussion started: 9 May 2023

the implemented general actuator disc (GAD) model (Mirocha et al., 2014; Kale et al., 2022) in WRF uses the AD+R method that is based on the BEM theory. However, the GAD requires high resolution, with at least a few grid points across the rotor disc (Mirocha et al., 2014), making the simulation costly for large arrays of turbines or multiple wind farms. Compared to the WFP approaches, the GAD model requires more information about the turbine, such as blade profiles and aerodynamic characteristics, as well as generator speed and blade pitch control. This information is sometimes confidential and not publically available. Finally, despite the open-source availability of the WRF, the source code for the GAD implementation has not been publicly released, limiting its use for the scientific community.

On the other hand, the implemented general actuator disc (GAD) model in WRF (Mirocha et al., 2014; Kale et al., 2022) employs the AD+R method based on the BEM theory. However, due to the requirement for high resolution, with at least a few grid points across the rotor disc, the simulation can become costly for large arrays of turbines or multiple wind farms. Additionally, the GAD model requires more information about the turbine, such as blade profiles and aerodynamic characteristics as well as generator speed and blade pitch control, which may sometimes be confidential and not publicly available. Finally, the GAD implementation's source code has not been released publicly, limiting its use for the scientific community, despite the WRF being open-source.

In this study, we developed a new wind turbine parameterization (WTP) model, named the Simple Actuator Disc for Large Eddy Simulation (SADLES), which is a compromise between the Generalized Actuator Disc (GAD) and Wind Farm Parameterization (WFP) models within the Weather Research and Forecasting (WRF) model. The purpose of this model is to simulate the turbine wake explicitly for intermediate resolutions between the GAD and WFP models, e.g. tens of meters. SADLES uses the AD method and requires only basic information about the turbines, such as their thrust and power curves, similar to the WFP model proposed by Fitch et al. (2012). To accommodate the Large Eddy Simulation (LES) downscaling approach, we also implemented the cell perturbation method (Muñoz-Esparza et al., 2014), which is necessary for generating turbulence in the nested domains. We integrated SADLES and the cell perturbation method as WRF modules and released the code as open-source with the aim of including the model in the official WRF repository for further open research.

To validate the WRF-SADLES model, we chose to compare its idealized simulations of a 5-MW wind turbine with similar simulations using the PALM model. The reason for selecting PALM was that it includes a wind turbine model (PALM-WTM) that uses the AD+R method, which is comparable with the AD method used by the WRF-SADLES, but with higher accuracy. Moreover, the PALM-WTM has been shown to agree well with more sophisticated wake models and observations (Witha et al., 2014; Vollmer et al., 2015; Bakhoday-Paskyabi et al., 2022a, b). In addition, we demonstrated a more realistic application of the WRF-SADLES by downscaling the ERA5 reanalysis data (Hersbach et al., 2020) to a 40-m resolution around the Alpha Ventus wind parks, enabling us to investigate the effects of turbine-to-turbine and farm-to-farm interactions.

The rest of the paper is organized as follows. Section 2 describes the implementation of the SADLES model. Section 3 describes an idealized simulation with a single 5-MW wind turbine and compares it with the PALM model. Section 4 provides an example application of a multi-scale down-scaling application with multiple wind farm simulations. Finally, Section 5 discusses the potential applications and limitations of the SADLES model.

https://doi.org/10.5194/egusphere-2023-491
Preprint. Discussion started: 9 May 2023

2 Methods

2.1 The simple actuator disc for large eddy simuation

The actuator disc (Anderson, 2020) is a hypothetical surface perpendicular to the wind flow that extracts energy continuously from the ambient wind through the work of the thrust force:

$$\mathbf{F}_T = -\frac{1}{2}\rho C_T |\mathbf{V_0}| \mathbf{V_0} A, \tag{1}$$

where ρ is the air density, A is the rotor area, C_T is the thrust coefficient, which is a function of the ambient (unperturbed) wind speed $|\mathbf{V_0}| = \sqrt{u_0^2 + v_0^2}$. The wind speed at the rotor, $\mathbf{V}$, is reduced by the axial induction factor a through the relation:

$$\mathbf{V} = \mathbf{V_0}(1-a). \tag{2}$$

The tendency terms of the thrust force are incorporated into the WRF model at the grid cells where the actuator disc intersects:

$$\left.\frac{\partial u}{\partial t}\right|_T = -\frac{1}{2} C_T |\mathbf{V_0}| u_0 \frac{\delta A}{\Delta x \Delta y \Delta z} \tag{3}$$

$$\left.\frac{\partial v}{\partial t}\right|_T = -\frac{1}{2} C_T |\mathbf{V_0}| v_0 \frac{\delta A}{\Delta x \Delta y \Delta z} \tag{4}$$

Where δA is the portion of the actuator disc area within the grid cell, Δx, Δy, and Δz are the grid sizes. We can shorten the formula by defining the area factor $F_A = \delta A/(\Delta x \Delta y \Delta z)$, which can be determined by performing a vertical and horizontal discretization of the actuator disc area (Fig. 1).

We note that in the WRF model, the tendency terms are defined for the coupled velocity, which is defined as $U = \mu_d u$, with μ_d is the dry mass of air column. It is also more convenient to use the wind speed at the rotor disc instead of the ambient wind speed. Thus the tendency terms to be added to the model become:

$$\left.\frac{\partial U}{\partial t}\right|_T = -\frac{1}{2(1-a)^2} \mu_d C_T |\mathbf{V}| u F_A \tag{5}$$

$$\left.\frac{\partial V}{\partial t}\right|_T = -\frac{1}{2(1-a)^2} \mu_d C_T |\mathbf{V}| v F_A \tag{6}$$

In contrast to the GAD model, the simple AD model does not explicitly represent the rotational effect. Instead, the rotational effect is treated as the subgrid-scale turbulence that affects the wake recovery. This effect is represented by adding a source of subgrid-scale turbulent kinetic energy (TKE), similar to the approach used in Fitch et al. (2012):

$$\left.\frac{\partial \mathrm{TKE}}{\partial t}\right|_T = \frac{1}{2(1-a)^3} \mu_d C_{TKE} |\mathbf{V}|^3 F_A \tag{7}$$

https://doi.org/10.5194/egusphere-2023-491
Preprint. Discussion started: 9 May 2023

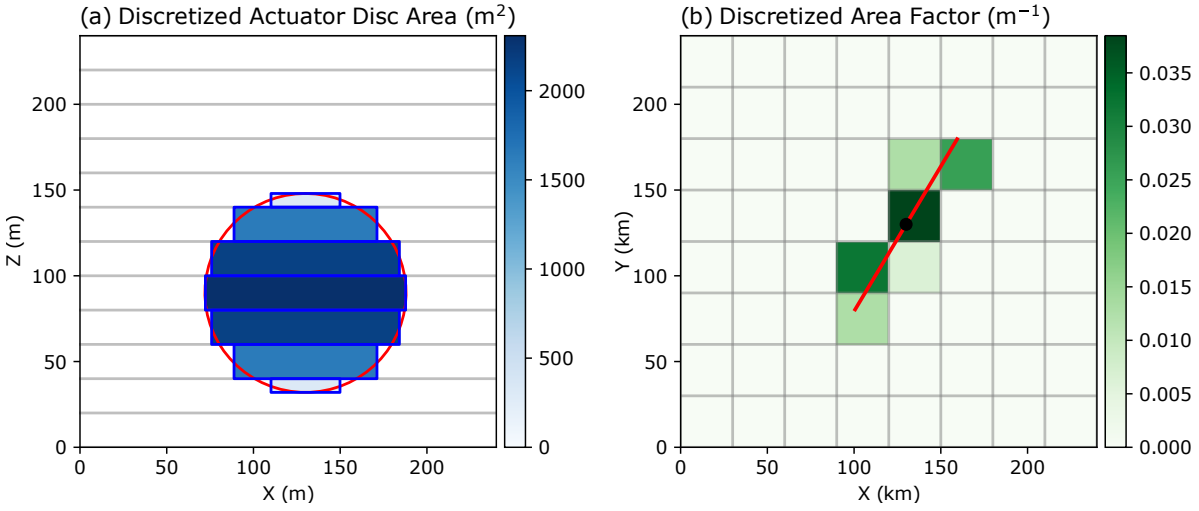

Figure 1. An example of vertical discretization (a) and horizontal discretization (b) of an actuator disc. The turbine radius is 58 m and the grid size is 30 m for both horizontal and vertical grids.

where $C_{TKE} = f_{TKE}(C_T - C_P)$, C_P is the power coefficient, and f_{TKE} is a factor that controls the amount of kinetic energy loss is converted to TKE.

The tendency terms above depend critically on the axial induction factor a. Some previous studies have used certain specific values of a, such as $a = 1/4$ (Calaf et al., 2010) or even $a = 0$ (Fitch et al., 2012) (i.e. they used the wind speed at the grid point directly instead of the unperturbed wind speed). In our implemented SADLES model, we provide two options for estimating a:

- Option 1 (direct evaluation): First, the hub-height ambient wind speed $|\mathbf{V}_0|$ is evaluated at two rotor diameters ($2D$) in front of the turbine. Then, the induction factor is calculated by:

  $a = 1 - \frac{|\mathbf{V}|}{|\mathbf{V_0}|}$,

  where $\mathbf{V}$ is the wind speed at the rotor location.

- Option 2 (inferred evaluation): In this option, only the hub-height wind speed at the rotor location is needed. Instead, we assume the 1-dimensional momentum theory ($C_T = 4a(1-a)$) and therefore:

  $a = \frac{1}{2}(1 - \sqrt{1 - C_T(|\mathbf{V}|)})$

  Note that although the thrust curve is typically provided as a relation between C_T and the ambient wind speed $|\mathbf{V}_0|$, we can also establish the relation between C_T and the wind speed at the rotor $|\mathbf{V}|$ using the 1-dimensional momentum theory.

In general, the direct evaluation of a (Option 1) should be more accurate. However, using this formula, a can exceed 0.5, which is nonphysical because it assumes that the wind behind the turbine becomes opposite the ambient wind. This can lead to

https://doi.org/10.5194/egusphere-2023-491
Preprint. Discussion started: 9 May 2023

model instability in some situations. Thus, the upper limit of a is set to the inferred evaluations of a (Option 2). In cases where the resolution is coarse, for example, a few hundred meters and the evaluation grid point may be at the same location as the turbine, the inferred evaluation (Option 2) may also be more appropriate.

2.2 Cell perturbation

Traditional LES simulations often use periodic lateral boundary conditions, which allow turbulent eddies to fully develop into a pseudo-equilibrium state. However, in our LES downscaling approach, the limited time and space available at the inflow boundary can prevent eddies from fully developing, particularly in cases with a small inner domain, high ambient wind speed, or stable boundary layer conditions. This can lead to incomplete development of the eddies and potentially affect the accuracy of the simulation.

The above problem can be alleviated using the cell perturbation method (Muñoz-Esparza et al., 2014, 2015), which is a simple and effective way to improve the realism of turbulent representations. The method adds a random perturbation of potential temperature within the interval [–0.5, 0.5] to three cells of 8×8 grid points near the chosen boundaries. In the idealized setup of Muñoz-Esparza et al. (2014), perturbations are introduced at every vertical grid point up to two-thirds of the inversion layer, which is known in the idealized setting. In our approach, the perturbations are applied with full magnitude up to a predefined vertical level k_1 and then gradually reduced to zero at a higher level k_2 using the weight $\cos^2[0.5\pi(k-k_1)/(k_2-k_1)]$, where k is the vertical level. As noted by Muñoz-Esparza et al. (2014), the perturbation process should not be done at every time step, but at an interval that is at least equal to the perturbation time scale, $T_s = 8\Delta x/U$, where U is the characteristic velocity scale and Δx is the horizontal grid spacing.

Because the cell perturbation method is not available with the distribution of WRF, we included our implementation within the distribution of SADLES.

2.3 Code implementation and turbine information

We have incorporated the SADLES code into the Advanced Research WRF (ARW), version4.3.1 with MPI support by adding two new Fortran 90 modules: a SADLES module (module_sadles.F) and a cell perturbation module (module_cellpert.F). To use the code, users can copy these modules and override few related files to the existing WRF file structure and recompile the model system. Table A1 and Table A2 provide information on the options available in the SADLES and cell perturbation modules. The modified WRF system can also be used to simulate turbine behavior in idealized experiments by additional namelist options to specify the Coriolis parameter and surface roughness length. The code has been made available as open-source to promote open research and we hope it will be included in the official WRF repository in the future. In the next section, we use the turbine information from Larsén and Fischereit (2021), which contains the locations, thrust curves, and powers curves of wind turbines of several wind farms in the North Sea.

https://doi.org/10.5194/egusphere-2023-491
Preprint. Discussion started: 9 May 2023

Table 1. Domain configurations for the idealized WRF (prefix W) and PALM (prefix P) experiments

Experiments	Domain	$N_x \times N_y \times N_z$	$\Delta x[m]$	Δt [s]	L_x [m]	L_y [m]
W30m_Opt1,W30m_Opt2	D01	$322 \times 163 \times 91$	90	1/2	28890	14490
	D02	$322 \times 163 \times 91$	30	1/6	9660	4860
W10m_Opt1,W10m_Opt2	D01	$322 \times 163 \times 91$	30	3/20	9660	4860
	D02	$448 \times 163 \times 91$	10	1/20	4470	1620
P30m	D01	$336 \times 172 \times 90$	90	1/2	30240	15480
	D02	$336 \times 192 \times 160$	30	1/6	10080	5760
P10m	D01	$336 \times 176 \times 160$	30	3/20	10080	5280
	D02	$432 \times 192 \times 150$	10	1/20	4320	1920

3 Example 1: Idealized simulation

3.1 Expriment design

To start, we conducted and compared idealized experiments involving a single 5-MW turbine using the WRF-SADLES and the PALM models. The simulations are performed at two resolution of 10 m (high resolution) and 30 m (target intermediate resolution).

WRF configurations

In this example, we performed four idealized experiments using WRF-SADLES included two different resolutions (10 m and 30 m) and two different options for evaluating the axial induction factor (SADLES Opt1 and Opt2, representing direct and inferred evaluations, respectively). The domain configurations for each experiment are summarized in Table 1. Each experiment utilized two nested domains, with the outer domain having a coarser resolution (30 m or 90 m) and using periodic boundary conditions on all sides, and the inner domains (10 m or 30 m) applying cell perturbation at the inflow boundary on the east side. All domains except the 10-m domain had an aspect ratio of 2:1. The 10-m domain had a longer aspect ratio of 2.76:1 to allow the turbulence and turbine wake to evolve over a longer distance.

The model top for all experiments is set at 1600 m, with an 800-m Rayleigh damping layer at the top with a coefficient of 0.2 s^{-1}. There is no vertical level stretching for the 30-m resolution experiments. In the case of the 10-m experiments, the vertical levels are stretched such that the near-surface vertical resolution is roughly 10 m. The initial potential temperature is 288 K from the surface up to 500 m, and then increases with a lapse rate of 1 K/100 m. We configured an idealized weak convective boundary layer with a surface turbulence heat flux of $\overline{(\theta' w')}_s = 0.02$ W m s^{-2}, similar to some previous studies (Muñoz-Esparza et al., 2014; Kale et al., 2022). After a spin-up time of 24 hours, which is performed for the outer domain only, a quasi-equilibrium, well-mixed boundary layer is established. In order to have the wind in the boundary layer roughly in

https://doi.org/10.5194/egusphere-2023-491
Preprint. Discussion started: 9 May 2023

the zonal direction, the geostrophic wind is set to rotate slightly to the left, specifically, $U_g = 9.91$ m s^{-1} and $V_g = -1.33$ m s^{-1}. After the spin-up time, both domains are integrated for 5 hours with a 1-minute output interval for the inner domain (D02) for further analysis.

In our idealized experiments, no moisture is initialized. Except for the surface layer, all other physical parameterization schemes, including microphysics, cumulus, boundary layer, and radiation, are turned off. For the surface layer parameterization, we used the Revised MM5 Monin-Obukhov surface layer scheme (Jiménez et al., 2012). Similar to the idealized experiment, to enable the LES mode, we used the 1.5-order three-dimensional LES turbulence closure, in which the sub-grid TKE is treated as a prognostic variable (Lilly, 1967). Other settings include: the Coriolis parameters are set to 1.177×10^{-4}s^{-1} (54°N), and the surface roughness length is set to 1 mm.

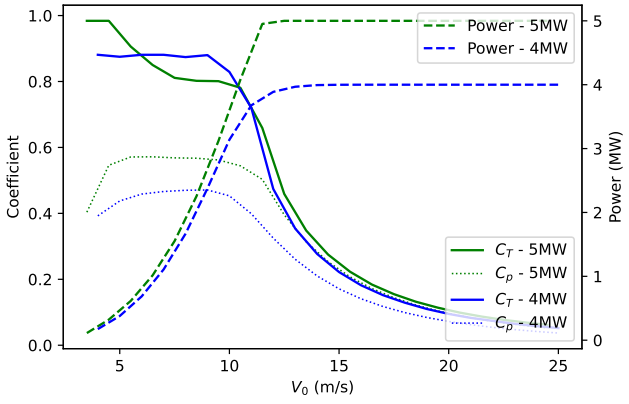

Figure 2. Power, thrust coefficient (C_t), and power coefficient (C_p) as functions of ambient wind speed (V_0) are shown for the 4 MW and 5 MW wind turbines used in the idealized (5 MW) and realistic (4 MW and 5 MW) experiments in this paper.

At the center of the inner domain, we placed a 5 MW wind turbine used at the Alpha Ventus wind farm. The turbine information taken from Larsén and Fischereit (2021) includes a rotor diameter of 116 m, a hub height of 90 m and the thrust and power coefficient curves at different wind speed (Fig. 2).

PALM configurations

To evaluate the performance of the SADLES module in simulating turbine wakes, we compared the results from the WRF-SADLES model with those from the Parallelized Large-eddy Simulation Model (PALM, Maronga et al., 2015, 2020), system 21.10 revision r4901. PALM is an LES model developed at Leibniz Universität Hannover, Germany, and has been shown in several studies to be capable of simulating wind turbine wakes effectively (e.g. Witha et al., 2014; Vollmer et al., 2015).

The wind turbine in PALM (PALM-WTM) is represented by an advanced actuator disc with rotation, which calculates both the thrust and torque force as a function of radius and tangential distance from the rotor center. Similar to the GAD methods (Mirocha et al., 2014; Kale et al., 2022), PALM-WTM computes the local lift and drag forces based on the Blade Element

https://doi.org/10.5194/egusphere-2023-491
Preprint. Discussion started: 9 May 2023

Momentum (BEM) method, which is accurate but requires additional information on the turbine and blade aerodynamic properties. For this reason, currently only two types of wind turbines are officially supported, including the National Renewable Energy Laboratory (NREL) 5-MW and 15-MW models (Jonkman et al., 2009; Gaertner et al., 2020). To compare with WRF-SADLES, we used the NREL 5-MW model with the same hub height of 90 m. However, the rotor diameter of the NREL 5-MW is slightly larger at 128 m compared to the 116 m diameter of the 5-MW turbine used in WRF-SADLES.

We design two idealized experiments, P10m and P30m, with two nested domains similar to the WRF experiments (see Table 1 for domains configurations). Cyclic lateral boundary conditions were used for the coarser domain. To prepare initial conditions for the main run we used a precursor run. Precursor domains are very smaller than main simulations. It has been defined 96×64 grid points for both 30m and 10m simulations in precursor run. Number of vertical levels for each precursor run is the same as the main run. The model has implemented for 86400 seconds to reach a steady state condition in precursor mode. To parameterize subgrid-scale (SGS) turbulence in PALM we used 1.5-order closure (according to Deardorff (1980) and modified by Moeng and Wyngaard (1988) and Saiki et al. (2000)). The same atmospheric conditions as the WRF model were considered. Initial potential temperature is 288 K, surface turbulence heat flux of $\overline{(\theta' w')_s} = 0.02$ W m s^{-2}, the geostrophic wind is about 10 m/s from the west.

3.2 Result

Figure 3 illustrates the instantaneous hub-height wind speed after 60 minutes of simulation for all experiments. In the 10-m resolution experiments, a distinct wake from the turbine is visible and is similar in both the PALM and WRF-SADLES experiments. The wake extends from the rotor and stretches over a distance of 1500 m (or 13 turbine diameters), exhibiting some small-scale meandering. Inside the wake, the wind speed drops to below 5 m/s, compared to the ambient wind speed of approximately 10 m/s outside of the wake. Compared to the 10-m resolution experiments, the wake is less clear in the 30-m resolution experiments. It also appears that the wake recovery is slower in the PALM experiment (P30m).

In both the PALM and WRF-SADLES experiments, there are elongated features that can be seen in the turbulence. However, there appears to be turbulent-free regions between these features in the PALM experiments, while there is intermediate turbulence present in between these features in the WRF-SADLES experiments. This is likely due to the cell perturbation at the inflow boundary, which causes the turbulence in the WRF-SADLES experiments to fully develop quickly before reaching the wind turbine located at the center of the domain.

The time-averaged power spectral densities (PSDs) of the two models (shown in Figure 4) are similar, particularly in the 10-m resolution experiments. In both models, the $-5/3$ Kolmogorov power law is only applicable to a short range of wave numbers (from 2×10^{-3} m^{-1} to $\times 10^{-2}$ m^{-1}, or wave lengths from 100 m to 500 m) for the 10-m experiments. In comparison, the 30-m resolution experiments have a higher PSD than the 10-m resolution experiments for wave numbers less than 3×10^{-3} m^{-1} (corresponding to wave lengths of about 300 m), but the PSDs quickly decrease for higher wave numbers.

There are some differences in the PSDs of the two models. One notable difference is that the PSDs of the WRF-SADLES decrease more quickly for wave numbers higher than 3×10^{-3} m^{-1} in the 30-m resolution experiments. Secondly, in the PALM experiments, the PSDs evaluated 1500 m behind the turbine are slightly higher than those evaluated 500 m in front of the

https://doi.org/10.5194/egusphere-2023-491
Preprint. Discussion started: 9 May 2023

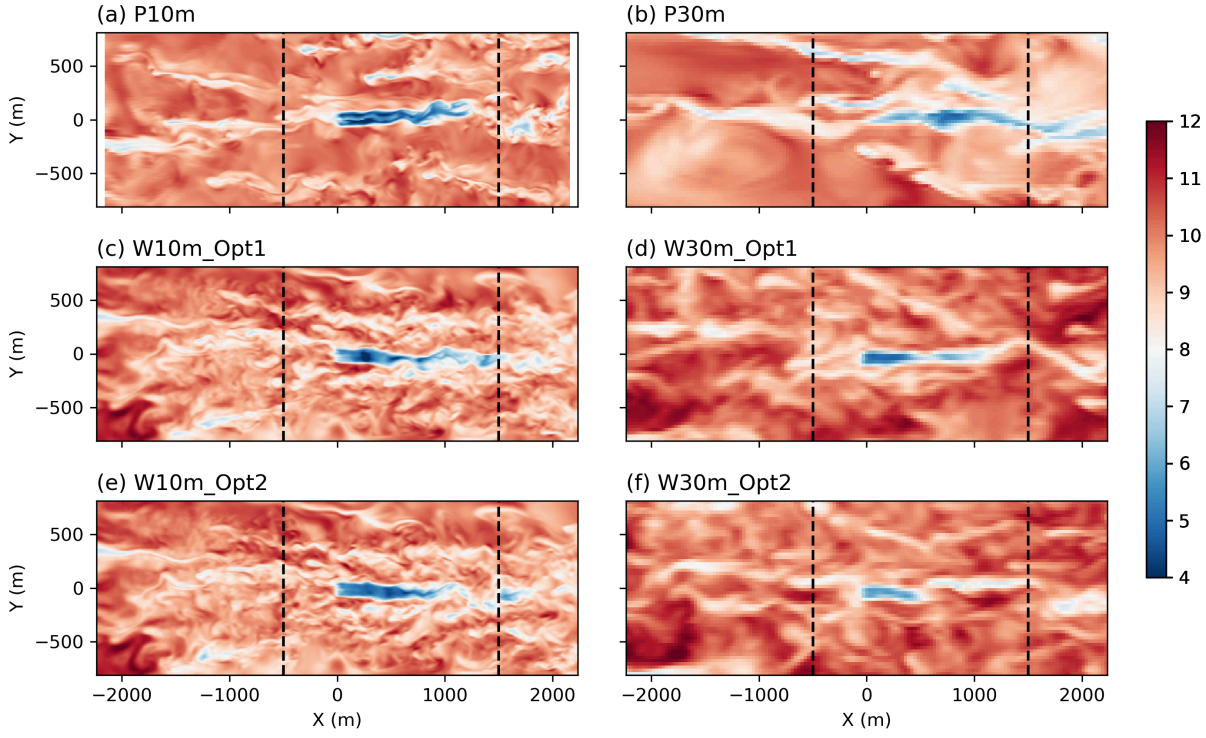

Figure 3. Snapshot at 60 minute of wind speed at turbine hub height (90 m) for idealized LES simulation using PALM (a,b) and WRF-SADLES (c,d-Option 1; e,f-Option 2) . For comparison, all the domains is zoomed to the WRF's 10-m resolution domain. The vertical dashed lines show the locations for the spectral analysis in Fig.4

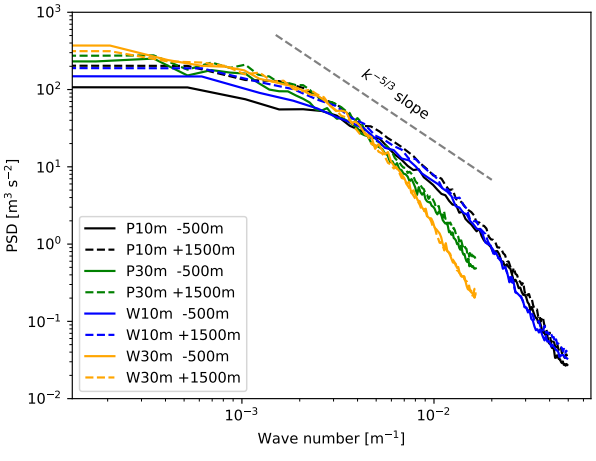

Figure 4. Power spectral density of wind speed for PALM and WRF-SADLES at 500m in front of the turbine (shown with solid lines) and 1500 m behind the turbine (shown with dashed lines).

https://doi.org/10.5194/egusphere-2023-491
Preprint. Discussion started: 9 May 2023

turbine, suggesting that the turbine model has increased the explicit turbulence. However, in the WRF-SADLES experiments, the turbine has little effect on the explicit turbulence due to the lack of consideration for tangential effects, as indicated by the small difference in the PSDs behind and in front of the turbine.

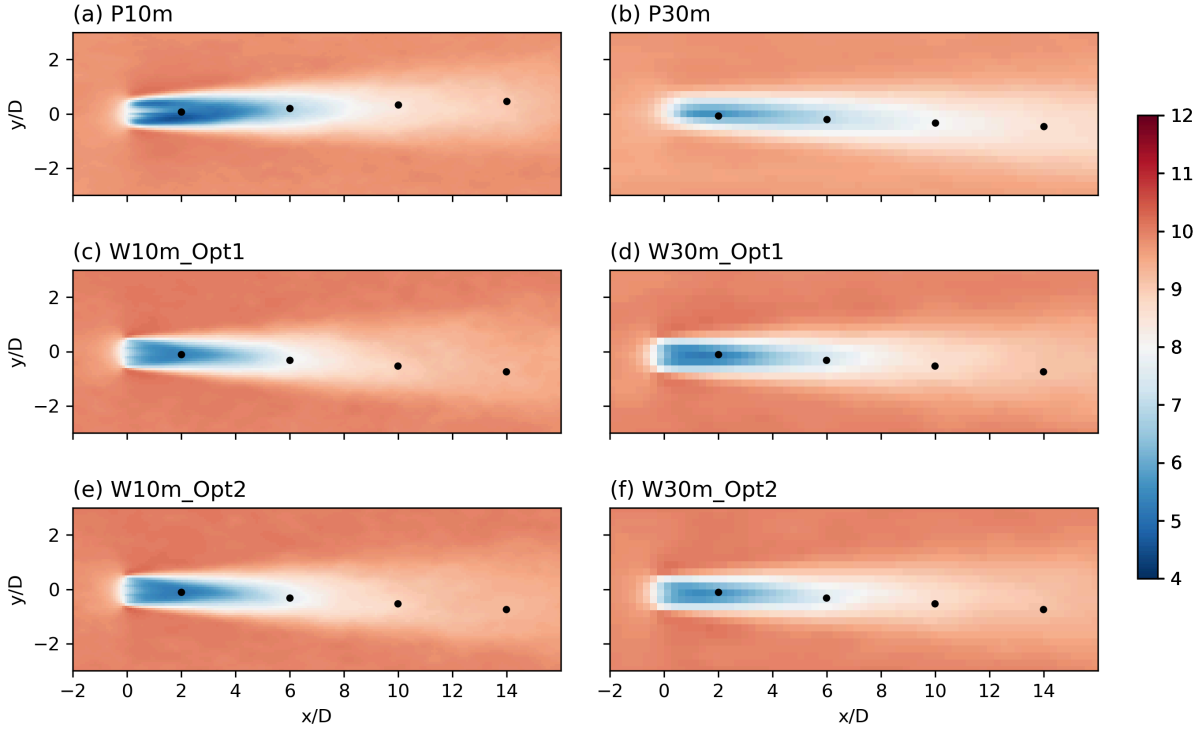

Figure 5. 4-hour average wind speeds at the turbine hub height (90 m) for idealized LES simulations using PALM (shown in panels a and b) and WRF-SADLES (shown in panels c and d for Option 1, and panels e and f for Option 2). The dots indicate the locations of 2D, 4D, 8D, and 12D, which are used for evaluating the wake deficit in Figure 6.

Figure 5 shows the average wind speeds over a 4-hour period for all of the idealized experiments. It can be seen that the averaged wakes are not perfectly aligned in the zonal (west-east) direction because the quasi-equilibrium states depend on the momentum fluxes of eddy activities, which may vary slightly between different models and resolutions. In the 10-m resolution experiments, the wake intensity appears to be slightly stronger in the PALM simulations compared to the WRF-SADLES simulations, which could be due to differences in the methods and turbine configurations used. However, when comparing the 30-m resolution simulations to the 10-m resolution simulations, the WRF-SADLES experiments show better agreement than the PALM experiments. The 30-m resolution simulation of PALM (shown in Figure 5b) has a less distinct, but longer, stretched wake. There is also good agreement between the two SADLES options (shown in Fig. 5c,d and Fig. 5e,f), which confirms the validity of the 1-D momentum theory.

https://doi.org/10.5194/egusphere-2023-491
Preprint. Discussion started: 9 May 2023

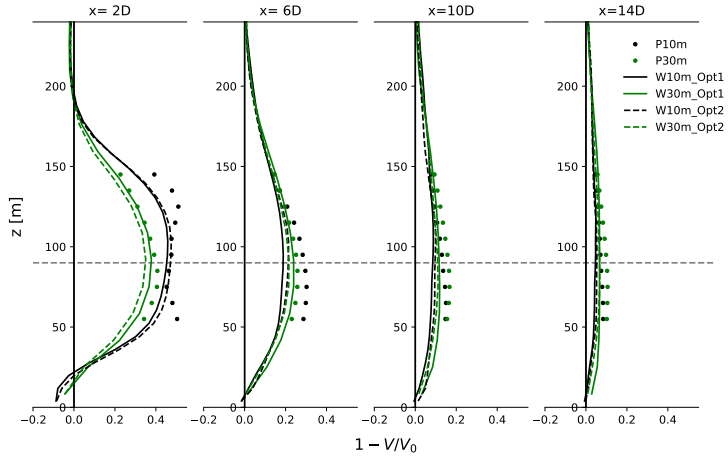

Figure 6. Vertical wake deficit $(1 - V/V_0)$ for idealized at distances behind the turbine of two turbine diameters $(2D)$, $6D$, $10D$, and $14D$. The evaluation points are indicated by black dots in Fig. 5.

We calculated the vertical wake deficit at distances behind the turbine of two turbine diameters $(2D)$, $6D$, $10D$, and $14D$ (as shown in Figure 6). The positions where the wake deficit was calculated are indicated by the black dots in Figure 5. Because the average wake axes are not perfectly aligned in the zonal direction, we did not use the (x, z)-cross section output of the PALM model, but instead calculated the wake deficit from the 3D outputs, which have limited vertical levels (shown by dots in Fig.6).

At the near-wake distance of two turbine diameters $(2D)$, for both PALM and WRF-SADLES, the wake 10-m simulations have a slightly stronger wake deficit compared to the 30-m simulations. However, the P10m has a lower deficit near the hub height because of the BEM method used in PALM. This feature does not present in WRF-SADLES and also in P30m because of the resolution limitation

At a distance of two turbine diameters from the turbine (near-wake), both the PALM and WRF-SADLES simulations with a 10-m resolution show a slightly stronger wake deficit compared to the simulations with a 30-m resolution. However, the PALM simulation with a 10-m resolution (P10m) has a lower deficit near the hub height, which is likely due to the BEM method used in PALM. This feature is not present in the WRF-SADLES simulations or in the PALM simulation with a 30-m resolution (P30m), which may be due to the resolution limitation. As the distance from the turbine increases, this feature disappears and the deficit shapes of the two models become similar. The wake deficit for the higher-resolution simulations (10-m) recovers faster than the lower-resolution simulations (30-m), which may be due to the effect of explicit turbulence, which is weaker for lower resolutions. However, at a far wake distance $(10D)$, the WRF-SADLES simulations of two resolutions agree slightly better than the PALM simulation, which is likely due to the sub-grid turbulent effects from the TKE production of SADLES.

Figure 7a shows the box plots of the ambient wind speeds for the WRF-SADLES experiments. For direct evaluation (Option 1) of the ambient wind speed, there is a slight difference of approximately 0.15 m/s in the average wind speed for the resolutions

https://doi.org/10.5194/egusphere-2023-491
Preprint. Discussion started: 9 May 2023

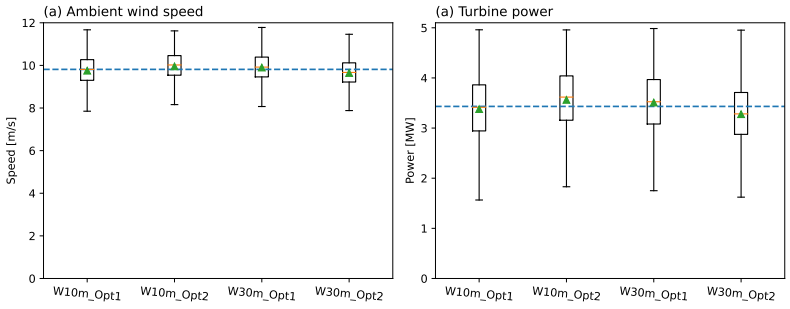

Figure 7. Box plots of ambient wind speed (a) and turbine power (b) for the WRF-SADLES experiments are shown. In each panel, the average of all experiments is indicated by a dashed line for comparison.

Table 2. WRF domain configurations for the real-data downscaling experiments.

Domain	$N_x \times N_y \times N_z$	Δx (m)	Δt [s]	L_x [km]	L_y [km]
D01	$385 \times 321 \times 60$	9000	45	3456	2880
D02	$481 \times 382 \times 60$	3000	15	1440	1143
D03	$322 \times 322 \times 60$	1000	5	321	321
D04	$321 \times 321 \times 60$	200	1	64	64
D05	$481 \times 481 \times 60$	40	1/5	19.2	19.2

of 10 m and 30 m. This is likely due to differences in eddy fluxes. When it comes to the inferred evaluation of the ambient wind speed (Option 2), the difference between the two resolutions is slightly larger, at about 0.3 m/s. Both of these differences are relatively small, representing about 1.5% and 3% of the ambient wind speed, respectively. However, due to the non-linear relationship, the differences in the turbine power (Figure 7b) are larger, at 4% for Option 1 and 8% for Option 2. Compared to the average wind speed and turbine power of Option 1 and Option 2, Option 2 is larger for the 10 m resolution, but smaller for the 30-m resolution.

4 Example 2: Real data meso-to-micro nesting simulation

4.1 Model configurations

In this example, we used the WRF-SADLES system to downscale the ERA5 global reanalysis data (Hersbach et al., 2020). The ERA5 data has a resolution of approximately 31 km and is available on an hourly basis. To achieve a turbine-scale resolution of 40 m, we used a system of five nested domains (as shown in Table 2). The outermost domain (D01) had a resolution of 9 km and covered a large region including Europe and the North-East Atlantic Ocean, while the second domain (D02) specifically

https://doi.org/10.5194/egusphere-2023-491
Preprint. Discussion started: 9 May 2023

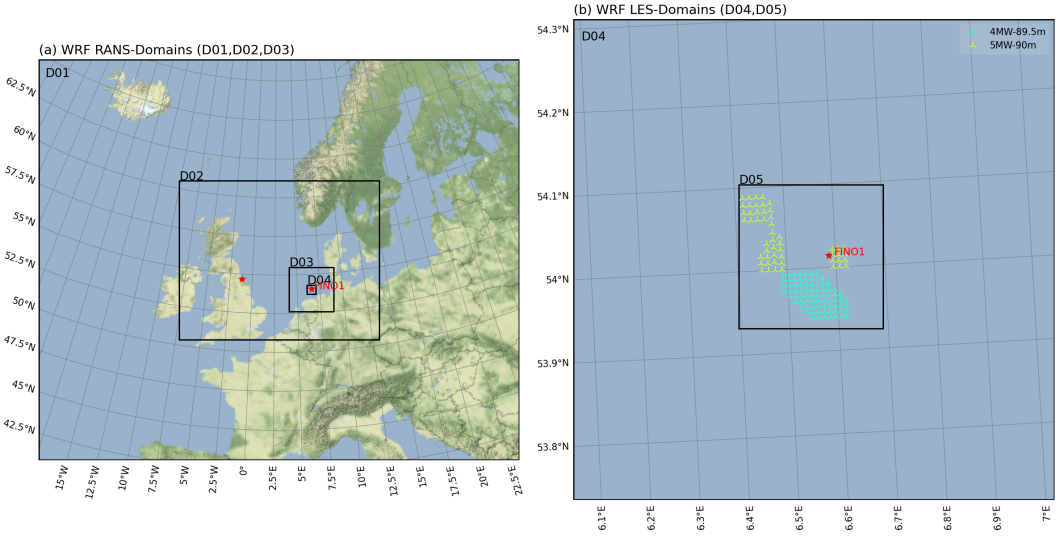

Figure 8. WRF domains used for example 2. The first three domains (a) are the mesoscale or Reynolds-averaged Navier–Stokes (RANS) domains. The two innermost domains (b) are the LES domains. See Table 2 for detailed domains dimensions. The terrain map was generated using data from Stamen Design with a Creative Commons Attribution (CC BY 3.0) license.

covered the North Sea (Figure 8a). The remaining domains were centered around the Alpha Ventus wind farm, located next to the FINO1 meteorological mast station (Figure 8b). The innermost domain (D05) had dimensions of 19.2 km × 19.2 km, which was smaller than a single grid cell of the original ERA5 data. For the vertical grid, we used 60 levels as in Bui and Bakhoday-Paskyabi (2022), allowing for high resolution near the surface of approximately 10 m and 21 levels below a height of 500 m.

In the innermost domain (Figure 8b), there are four wind farms consisting of 5-MW and 4-MW turbines. Notably, the Alpha Ventus wind farm with twelve turbines is located to the right of the Fino1 mast station. The detailed turbine specifications, such as power and thrust curves, can be found in Larsén and Fischereit (2021) (see Fig. 2).

The LES simulations were performed for domains D04 and D05 from 06Z to 12Z September 24, 2016. The mesoscale domains began earlier at 00Z September 23 to spin up the environmental conditions. This period was chosen due to relatively steady winds from the South-Southwest direction, which allows for both turbine-to-turbine (intra-farm) and farm-to-farm interactions to occur within the Alpha Ventus wind farm. Thus, we designed two experiments where the SADLES Option 1 is applied for the innermost (40-m) domain: the first experiment (EXP1) includes all four wind farms, while the second experiment (EXP2) removes all wind farms except Alpha Ventus. This experimental design allows us to quantify the influence of the wind farm to the southwest of Alpha Ventus on the wind farm.

In this study, specific physical options are chosen as follows. The RRTMG (Rapid Radiative Transfer Model for General Circulation Models) scheme (Iacono et al., 2008) is used for the radiation parameterization in all domains, and the Thompson graupel scheme (Thompson et al., 2008) is used for microphysics parameterization. The Tiedtke scheme (Zhang et al., 2011)

https://doi.org/10.5194/egusphere-2023-491
Preprint. Discussion started: 9 May 2023

is used for the cumulus parameterization in the outermost 9-km domain (D01), while cumulus parameterization is turned off in all other domains with finer resolutions. The Monin-Obukhov Similarity scheme (Jiménez et al., 2012) is used for surface layer parameterization and the Noah Land Surface Model (Mukul Tewari et al., 2004) is used for land surface parameterization in all domains. The Yonsei University (YSU) scheme (Hong et al., 2006) is used for PBL parameterization in the mesoscale domains (D01-D03), while PBL parameterization is turned off in the LES (Large Eddy Simulation) domains (D04, D05). The 1.5-order three-dimensional TKE closure (Lilly, 1967) is used for simulating large eddies in the LES domains, and the cell perturbation method is applied to the southern and western boundaries for the first 16 levels from the surface (to a height of about 300 m) to trigger the development of turbulence.

4.2 Result

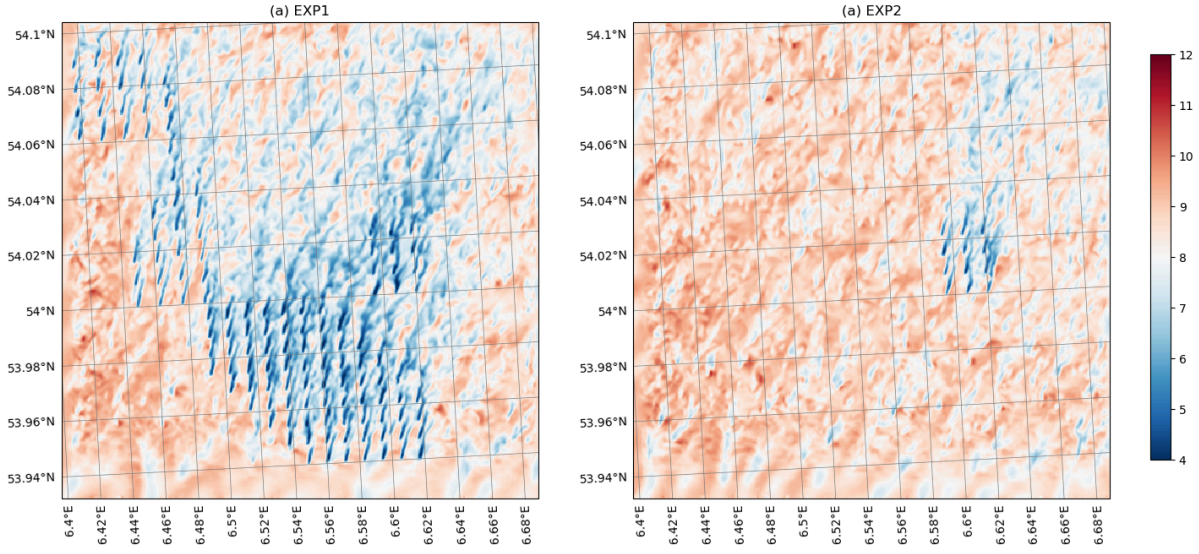

Figure 9. The instantaneous wind speed in the 40-m domain (D05) at a height of 90 meters at 08Z on September 24, 2016, for the two experiments in Example 2.

Figure 9 shows an example snapshot of the wind speed at the Alpha Ventus hub-height (90 m) for the 40-m LES domain for the two experiments at 08Z on September 24, 2016. Thanks to the cell perturbation at the southern boundary, the turbulence quickly becomes fully developed after about two kilometers (or roughly ten percent of the domain width) from the border. This allows the turbulence flow to become quasi-steady when it reaches the turbines in the wind farms. Such turbulence development is important because it affects the wake recovery behind the turbines.

At the current time, the ambient wind speed is about 9 m/s, and the turbine wakes are clearly visible with a speed reduced to less than 5 m/s. The individual wakes have a stretch of about two kilometers. However, the imprint of the collective effect of the wind farm extends much further, covering more than half of the domain (or over ten kilometers). This collective effect of

https://doi.org/10.5194/egusphere-2023-491
Preprint. Discussion started: 9 May 2023

the wind farm to the southwest of Alpha Ventus (Fig. 9) reduces the speed of the ambient flow compared to the case without the southwest wind farm. Thus we expect this farm-to-farm effects should reduce the extracted power of the Alpha Ventus.

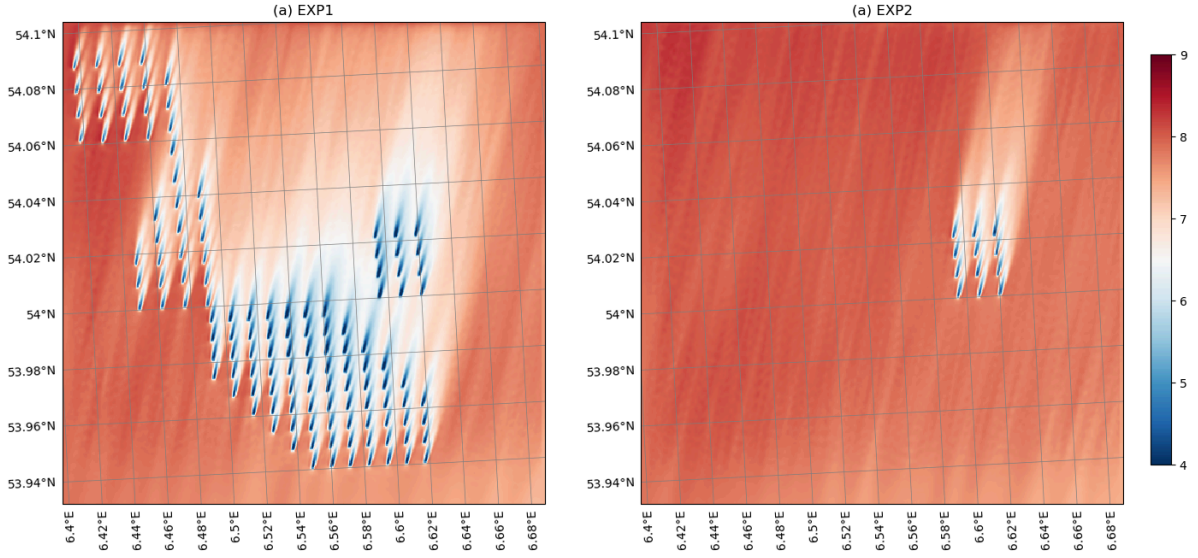

Figure 10. The 5-hour average wind speed (from 07Z to 12Z on September 24, 2016) for the 40-m domain at a height of 90 meters for the two experiments in Example 2.

The five-hour average wind speed (from 07Z to 12Z on September 24, 2016) shows that the ambient wind is relatively steady during this period with an average wind speed of about 8 m/s when it enters the domain D05 (Fig. 11). Because of the south-southwest wind direction, the wake caused by the southwest wind farm causes the average wind speed to reduce to about 6–7 m/s before it reaches the Alpha Ventus wind farm. This causes the Alpha Ventus wakes to become more visible in the case of EXP1 (with nearby wind farms) compared with EXP2 (without nearby wind farms). However, the effect of the intra-farm interaction within the Alpha Ventus due to the wakes does not directly align with the downstream turbines of the next row.

The box plots in Fig. 11 also show that there is little intra-farm interaction in the wind speeds experienced by the turbines. In the EXP1 experiments, there is no evidence of the wind speeds being reduced by the turbines in the rows at the back. In fact, turbine T1 has the lowest average ambient wind speed, which may be due to the wake from a turbine in the southwest wind farm (see Fig. 11a). Similarly, in the EXP2 experiments, the ambient wind speeds for each turbine are similar except for turbines T11 and T12 at the back row. These turbines likely experience a reduction in wind speed due to the average wakes from turbines T1 and T2 in the front row, rather than from the row directly in front of them (see Fig. 11b).

The average ambient wind speed at the Alpha Ventus wind farm is lower when there are nearby wind farms present compared to when there are none. When nearby wind farms (EXP1) are present, the average ambient wind speed is 6.5 m/s, as shown in Fig. 11a. In contrast, when there are no nearby wind farms (EXP2), the average ambient wind speed is 7.6 m/s, as shown in Fig. 11b. This represents a reduction in wind speed of about 14%. However, due to the non-linear nature of the turbine

https://doi.org/10.5194/egusphere-2023-491
Preprint. Discussion started: 9 May 2023

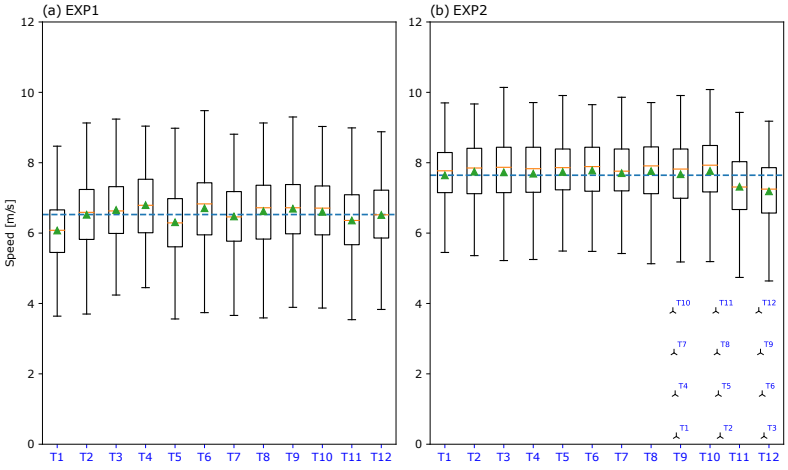

Figure 11. Box plots of 5-hour ambient wind speeds (from 07Z to 12Z on September 24, 2016) for the turbines in the Alpha Ventus wind farm. The average values (blue dashed lines) are 6.5 m/s and 7.6 m/s for (a) and (b) respectively. The layout of the turbines in the Alpha Ventus wind farm is shown on the bottom right of panel (b).

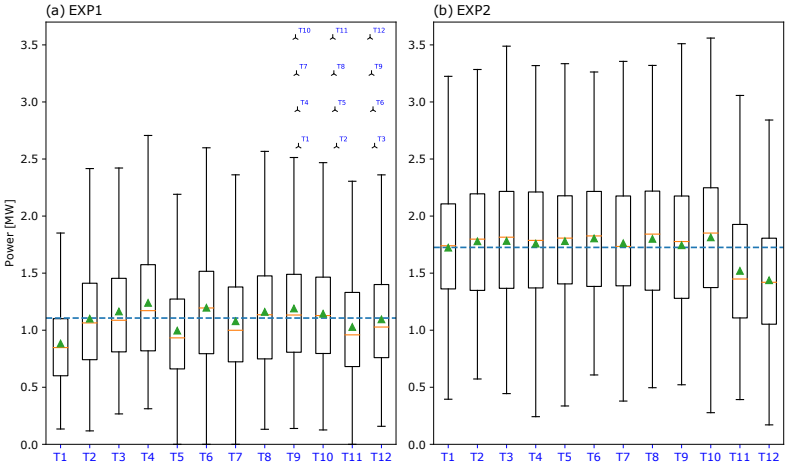

Figure 12. Similar to Fig. 11, but for turbine powers. The average values (blue dashed lines) are 1.1 MW and 1.7 MW for (a) and (b) respectively.

https://doi.org/10.5194/egusphere-2023-491
Preprint. Discussion started: 9 May 2023

power curve, the power reduction resulting from the farm-to-farm interaction (Fig. 12) is larger. The average power for EXP2 is approximately 1.7 MW, while the average power for EXP1 is 1.1 MW, corresponding to a reduction of about 35%.

5 Summary and discussion

In this paper, we present our implementation of a simple actuator disc model for large eddy simulation (SADLES) within the Weather Research and Forecast (WRF) model. Unlike other previous implementations of wind turbine parameterization within WRF, such as the General Actuator Disc (GAD) (Mirocha et al., 2014; Kale et al., 2022), SADLES only requires the power curve and thrust coefficient curve—the same information used in wind farm parameterization (WFP Fitch et al., 2012) that is already included in WRF. The purpose of SADLES is to explicitly simulate the wakes of multiple wind farms in online nested downscaling applications from realistic atmospheric conditions. The target resolution of the WRF-SADLES is the intermediate between the GAD model and the WFP, in which one turbine is represented by a few grid points.

SADLES uses the traditional actuator disc model, where the turbine is represented by a thin disc that causes a thrust force that slows down the ambient wind speed. A caveat of this method is the assumption of a uniform thrust coefficient for the actuator disc, and the lack of tangential velocity tendency and explicit turbulence behind the wind turbine, as demonstrated in our idealized experiment with a single 5-MW turbine (Section 3). However, the generated turbulence is still represented implicitly as the production of turbulent kinetic energy, which affects eddy diffusivity. When compared to a dedicated LES model (the PALM model), the simulated wake using WRF-SADLES has better agreement between the 30-m and 10-m resolutions.

We also demonstrate the application of SADLES using a real-data simulation (Section 4) that downscales a realistic dataset (ERA5 data) from a coarse resolution (about 31 km) to a turbine scale resolution (40 m). The downscaling is performed using a system of five nested domains, with the outer three domains simulating mesoscale processes and the two inner domains simulating eddy turbulence. In our specific experiment, we found little influence between the turbines within the Alpha Ventus wind farm, while the main influence is from the wind farm to the southwest. The presence of this wind farm reduces the ambient wind speed by about 14% and the average turbine power by 35%.

We have published our code as open source to encourage further open research in the field of wind energy. Our code distribution also includes our implementation of the cell perturbation method (Muñoz-Esparza et al., 2014), which is essential for the turbulence development in nested LES. It should be noted that SADLES is currently limited by the assumption of a disc always being perpendicular to the ambient flow, so wake deflection cannot currently be simulated. Some potential areas for further development of SADLES include the investigation of the TKE factor in wake representation and the inclusion of a parameterized net-tangential velocity tendency, which would enable the investigation of the turbine yaw control. In this study, we validated the WRF-SADLES model against another LES model, but further comparisons with observational data are necessary to fully verify the model's accuracy.

https://doi.org/10.5194/egusphere-2023-491
Preprint. Discussion started: 9 May 2023

Appendix A: Additonal WRF namelist options

Table A1. Summary of SADLES namelist options

Namelist options (`&physics`)	Default value	Description
`sadles_opt` (max_domains)	0	=0 turn off SADLES for the current domain; =1 or 2: use Option 1 (direct) or Option 2 (inferred) for the induction factor, respectively
`sadles_startmin` (max_domains)	0	Time to start SADLES in minutes
`sadles_maxradius` *	120	Max turbine radius in meter,
`sadles_mindx` *	20	Min Δx in meter,
`sadles_mindz` *	20	Min Δz in meter,
`sadles_tkefact`	0.5	f_{KTE}, from 0 to 1 (see the text for the description)
`ideal_f`	0.0001	Coriolis force (`em_les` only),
`ideal_znt`	-1.	Surface roughness length (`em_les` only, only effective for positive values).

* These values are used to allocate arrays within the SADLES module.

https://doi.org/10.5194/egusphere-2023-491
Preprint. Discussion started: 9 May 2023

Table A2. Summary of cell perturbation namelist options

Namelist options (`&cpert`)	Default value	Description
`cell_pert_xs` (max_domains)	0	=1 will apply cell perturbation for the western boundary
`cell_pert_xe` (max_domains)	0	=1 will apply cell perturbation for the eastern boundary
`cell_pert_ys` (max_domains)	0	=1 will apply cell perturbation for the southern boundary
`cell_pert_ye` (max_domains)	0	=1 will apply cell perturbation for the northern boundary
`cell_pert_magnitude`	0.5	Magnitude of the cell perturbation
`cell_pert_interval` (max_domains) *	320	Interval to apply the perturbation in seconds
`cell_pert_k1`	8	Bottom level of the transition layer for cell perturbation
`cell_pert_k2`	16	Top level of the transition layer for cell perturbation

* The interval should be approximately $\frac{8\Delta x}{U}$, where U is the average wind speed during the simulation. For example, with $\Delta x = 200$ m and $U = 5$ m/s, the interval will be approximately $\frac{8(200\text{ m})}{5\text{ m/s}} = 320$ s.

https://doi.org/10.5194/egusphere-2023-491
Preprint. Discussion started: 9 May 2023

Code and data availability.

Our WRF-SADLES initial released code with an example idealized settings for the 30-m simulation can be downloaded from: https://doi.org/10.5281/zenodo.7896366 (Bui, 2023). A short WRF-SADLES user's guide can be obtained from WRF-SADLES's Github repository: https://github.com/haibuihoang/WRF-SADLES. The WRF-ARW model can be downloaded from: https://github.com/wrf-model/WRF. The PALM model can be downloaded from: https://gitlab.palm-model.org/releases/palm_model_system. The ERA5 hourly reanalysis can be download from: https://cds.climate.copernicus.eu/. The information of turbines can be downloaded from: https://doi.org/10.5281/zenodo.4668613 (Larsén and Fischereit, 2021).

Author contributions. Hai Bui proposed and implemented the SADLES method, conducted the WRF-SADLES simulation, and wrote the manuscript. Mostsafa provided turbine information, revised the manuscript, and assisted with several technical discussions. Mohammadreza contributed by writing the description of the PALM model, performing the PALM simulation, and assisting with manuscript revisions.

Competing interests.

All authors declare that they have no competing of interest.

Acknowledgements. The work a part of the HIghly advanced Probabilistic design and Enhanced Reliability methods for high-value, cost-efficient offshore WIND (HIPERWIND) project, which has received funding from the European Union's Horizon 2020 Research and Innovation Programme under Grant Agreement No. 101006689. The simulations were performed on resources provided by project NN9871K by UNINETT Sigma2 - the National Infrastructure for High Performance Computing and Data Storage in Norway.

https://doi.org/10.5194/egusphere-2023-491
Preprint. Discussion started: 9 May 2023

References

Anderson, C.: Wind turbines: Theory and practice, Cambridge University Press, 2020.

Bakhoday-Paskyabi, M., Bui, H., and Mohammadpour Penchah, M.: Atmospheric-Wave Multi-Scale Flow Modelling, Deliverable D2.1 for HIPERWIND project, https://www.hiperwind.eu/, 2022a.

Bakhoday-Paskyabi, M., Krutova, M., Bui, H., and Ning, X.: Multiscale Simulation of Offshore Wind Variability During Frontal Passage: Brief Implication on Turbines' Wakes and Load, in: Journal of Physics: Conference Series, vol. 2362, p. 012003, IOP Publishing, 2022b.

Baldauf, M., Seifert, A., Förstner, J., Majewski, D., Raschendorfer, M., and Reinhardt, T.: Operational convective-scale numerical weather prediction with the COSMO model: Description and sensitivities, Monthly Weather Review, 139, 3887–3905, 2011.

Breton, S.-P., Sumner, J., Sørensen, J. N., Hansen, K. S., Sarmast, S., and Ivanell, S.: A survey of modelling methods for high-fidelity wind farm simulations using large eddy simulation, Philosophical Transactions of the Royal Society A: Mathematical, Physical and Engineering Sciences, 375, 20160 097, 2017.

Bui, H.: Simple Actuator Disc for Large Eddy Simulation (SADLES), https://doi.org/10.5281/zenodo.7896366, 2023.

Bui, H. and Bakhoday-Paskyabi, M.: Mesoscale Simulation of Open Cellular Convection: Roles of Model Resolutions and Physics Parameterizations, in: Journal of Physics: Conference Series, vol. 2362, p. 012006, IOP Publishing, 2022.

Burton, T., Jenkins, N., Sharpe, D., and Bossanyi, E.: Wind energy handbook, John Wiley & Sons, 2011.

Calaf, M., Meneveau, C., and Meyers, J.: Large eddy simulation study of fully developed wind-turbine array boundary layers, Physics of fluids, 22, 015 110, 2010.

Churchfield, M., Wang, Q., Scholbrock, A., Herges, T., Mikkelsen, T., and Sjöholm, M.: Using high-fidelity computational fluid dynamics to help design a wind turbine wake measurement experiment, in: Journal of Physics: Conference Series, vol. 753, p. 032009, IOP Publishing, 2016.

Deardorff, J. W.: Stratocumulus-capped mixed layers derived from a three-dimensional model, Boundary-layer meteorology, 18, 495–527, 1980.

Fischereit, J., Brown, R., Larsén, X. G., Badger, J., and Hawkes, G.: Review of Mesoscale Wind-Farm Parametrizations and Their Applications, Boundary-Layer Meteorology, 182, 175–224, 2022.

Fitch, A. C., Olson, J. B., Lundquist, J. K., Dudhia, J., Gupta, A. K., Michalakes, J., and Barstad, I.: Local and mesoscale impacts of wind farms as parameterized in a mesoscale NWP model, Monthly Weather Review, 140, 3017–3038, 2012.

Fleming, P. A., Gebraad, P. M., Lee, S., van Wingerden, J.-W., Johnson, K., Churchfield, M., Michalakes, J., Spalart, P., and Moriarty, P.: Evaluating techniques for redirecting turbine wakes using SOWFA, Renewable Energy, 70, 211–218, 2014.

Gaertner, E., Rinker, J., Sethuraman, L., Zahle, F., Anderson, B., Barter, G. E., Abbas, N. J., Meng, F., Bortolotti, P., Skrzypinski, W., et al.: IEA wind TCP task 37: definition of the IEA 15-megawatt offshore reference wind turbine, Tech. rep., National Renewable Energy Lab.(NREL), Golden, CO (United States), 2020.

Göçmen, T., Van der Laan, P., Réthoré, P.-E., Diaz, A. P., Larsen, G. C., and Ott, S.: Wind turbine wake models developed at the technical university of Denmark: A review, Renewable and Sustainable Energy Reviews, 60, 752–769, 2016.

Hersbach, H., Bell, B., Berrisford, P., Hirahara, S., Horányi, A., Muñoz-Sabater, J., Nicolas, J., Peubey, C., Radu, R., Schepers, D., et al.: The ERA5 global reanalysis, Quarterly Journal of the Royal Meteorological Society, 146, 1999–2049, 2020.

Hong, S.-Y., Noh, Y., and Dudhia, J.: A new vertical diffusion package with an explicit treatment of entrainment processes, Mon. Weather Rev., 134, 2318–2341, 2006.

https://doi.org/10.5194/egusphere-2023-491
Preprint. Discussion started: 9 May 2023

Iacono, M. J., Delamere, J. S., Mlawer, E. J., Shephard, M. W., Clough, S. A., and Collins, W. D.: Radiative forcing by long-lived greenhouse gases: Calculations with the AER radiative transfer models, J. Geophys. Res. Atmos., 113, 2008.

Jiménez, P. A., Dudhia, J., González-Rouco, J. F., Navarro, J., Montávez, J. P., and García-Bustamante, E.: A revised scheme for the WRF surface layer formulation, Monthly weather review, 140, 898–918, 2012.

Jonkman, J., Butterfield, S., Musial, W., and Scott, G.: Definition of a 5-MW reference wind turbine for offshore system development, Tech. rep., National Renewable Energy Lab.(NREL), Golden, CO (United States), 2009.

Kale, B., Buckingham, S., van Beeck, J., and Cuerva-Tejero, A.: Implementation of a generalized actuator disk model into WRF v4. 3: A validation study for a real-scale wind turbine, Renewable Energy, 197, 810–827, 2022.

Larsén, X. G. and Fischereit, J.: A case study of wind farm effects using two wake parameterizations in WRF (V3.7.1) in the presence of low level jets, https://doi.org/10.5281/zenodo.4668613, 2021.

Lee, J. C. and Lundquist, J. K.: Evaluation of the wind farm parameterization in the Weather Research and Forecasting model (version 3.8. 1) with meteorological and turbine power data, Geoscientific Model Development, 10, 4229–4244, 2017.

Lilly, D. K.: The representation of small-scale turbulence in numerical simulation experiments, IBM Form, pp. 195–210, 1967.

Lin, D., Khan, B., Katurji, M., Bird, L., Faria, R., and Revell, L. E.: WRF4PALM v1. 0: a mesoscale dynamical driver for the microscale PALM model system 6.0, Geoscientific Model Development, 14, 2503–2524, 2021.

Maronga, B., Gryschka, M., Heinze, R., Hoffmann, F., Kanani-Sühring, F., Keck, M., Ketelsen, K., Letzel, M. O., Sühring, M., and Raasch, S.: The Parallelized Large-Eddy Simulation Model (PALM) version 4.0 for atmospheric and oceanic flows: model formulation, recent developments, and future perspectives, Geoscientific Model Development, 8, 2515–2551, 2015.

Maronga, B., Banzhaf, S., Burmeister, C., Esch, T., Forkel, R., Fröhlich, D., Fuka, V., Gehrke, K. F., Geletič, J., Giersch, S., et al.: Overview of the PALM model system 6.0, Geoscientific Model Development, 13, 1335–1372, 2020.

Mirocha, J., Kosovic, B., Aitken, M., and Lundquist, J.: Implementation of a generalized actuator disk wind turbine model into the weather research and forecasting model for large-eddy simulation applications, Journal of Renewable and Sustainable Energy, 6, 013 104, 2014.

Moeng, C.-H. and Wyngaard, J. C.: Spectral analysis of large-eddy simulations of the convective boundary layer, Journal of Atmospheric Sciences, 45, 3573–3587, 1988.

Mukul Tewari, N., Tewari, M., Chen, F., Wang, W., Dudhia, J., LeMone, M., Mitchell, K., Ek, M., Gayno, G., Wegiel, J., et al.: Implementation and verification of the unified NOAH land surface model in the WRF model (Formerly Paper Number 17.5), in: Proceedings of the 20th Conference on Weather Analysis and Forecasting/16th Conference on Numerical Weather Prediction, Seattle, WA, USA, vol. 14, 2004.

Muñoz-Esparza, D., Kosović, B., Mirocha, J., and van Beeck, J.: Bridging the transition from mesoscale to microscale turbulence in numerical weather prediction models, Boundary-layer meteorology, 153, 409–440, 2014.

Muñoz-Esparza, D., Kosović, B., Van Beeck, J., and Mirocha, J.: A stochastic perturbation method to generate inflow turbulence in large-eddy simulation models: Application to neutrally stratified atmospheric boundary layers, Phys. Fluids, 27, 035 102, 2015.

Onel, H. C. and Tuncer, I. H.: Short-Term Numerical Forecasting of Near-Ground Wind Fields Using OpenFOAM Coupled With WRF, in: AIAA SCITECH 2023 Forum, p. 1737, 2023.

Porté-Agel, F., Bastankhah, M., and Shamsoddin, S.: Wind-turbine and wind-farm flows: A review, Boundary-layer meteorology, 174, 1–59, 2020.

Pryor, S. C., Shepherd, T. J., Volker, P. J., Hahmann, A. N., and Barthelmie, R. J.: "Wind Theft" from onshore wind turbine arrays: sensitivity to wind farm parameterization and resolution, Journal of Applied Meteorology and Climatology, 59, 153–174, 2020.

https://doi.org/10.5194/egusphere-2023-491
Preprint. Discussion started: 9 May 2023

Saiki, E. M., Moeng, C.-H., and Sullivan, P. P.: Large-eddy simulation of the stably stratified planetary boundary layer, Boundary-Layer Meteorology, 95, 1–30, 2000.

Salim, M. H., Schlünzen, K. H., Grawe, D., Boettcher, M., Gierisch, A. M., and Fock, B. H.: The microscale obstacle-resolving meteorological model MITRAS v2. 0: model theory, Geoscientific Model Development, 11, 3427–3445, 2018.

Skamarock, W. C., Klemp, J. B., Dudhia, J., Gill, D. O., Liu, Z., Berner, J., Wang, W., Powers, J. G., Duda, M. G., Barker, D. M., et al.: A description of the advanced research WRF model version 4, National Center for Atmospheric Research: Boulder, CO, USA, 145, 145, 2019.

Thompson, G., Field, P. R., Rasmussen, R. M., and Hall, W. D.: Explicit forecasts of winter precipitation using an improved bulk microphysics scheme. Part II: Implementation of a new snow parameterization, Mon. Weather Rev., 136, 5095–5115, 2008.

Volker, P., Badger, J., Hahmann, A. N., and Ott, S.: The Explicit Wake Parametrisation V1. 0: a wind farm parametrisation in the mesoscale model WRF, Geoscientific Model Development, 8, 3715–3731, 2015.

Vollmer, L., van Dooren, M., Trabucchi, D., Schneemann, J., Steinfeld, G., Witha, B., Trujillo, J., and Kühn, M.: First comparison of LES of an offshore wind turbine wake with dual-Doppler lidar measurements in a German offshore wind farm, in: Journal of Physics: Conference Series, vol. 625, p. 012001, IOP Publishing, 2015.

Wang, Q., Luo, K., Yuan, R., Wang, S., Fan, J., and Cen, K.: A multiscale numerical framework coupled with control strategies for simulating a wind farm in complex terrain, Energy, 203, 117 913, 2020.

Witha, B., Steinfeld, G., and Heinemann, D.: High-resolution offshore wake simulations with the LES model PALM, in: Wind energy-impact of turbulence, pp. 175–181, Springer, 2014.

Zhang, C., Wang, Y., and Hamilton, K.: Improved representation of boundary layer clouds over the southeast Pacific in ARW-WRF using a modified Tiedtke cumulus parameterization scheme, Mon. Weather Rev., 139, 3489–3513, 2011.